


# Combining the color structures and intersection points of thick center vortices and low-lying Dirac modes

Seyed Mohsen Hosseini Nejad\*

*Faculty of Physics, Semnan University, P.O. Box 35131-19111, Semnan, Iran*

 (Received 21 December 2017; revised manuscript received 20 February 2018; published 30 March 2018)

We investigate several examples of Yang-Mills gauge configurations containing center vortex structures, including intersection points between vortices and nontrivial color structures residing on the vortex world surfaces. Various topological charge contributions of the color structures and intersection points are studied in these configurations. Low-lying eigenmodes of the (overlap) Dirac operator in the presence of these vortex backgrounds are analyzed. The results indicate characteristic properties for spontaneous chiral symmetry breaking.

DOI: [10.1103/PhysRevD.97.054516](https://doi.org/10.1103/PhysRevD.97.054516)

## I. INTRODUCTION

Numerical simulations have indicated that the center vortices can account for the phenomena of the color confinement [1–9] and spontaneous chiral symmetry breaking [10–14]. Center vortices can contribute to the topological charge through intersection and writhing points [14–24] and their color structure [22,24–28]. We have studied colorful plane vortices in Refs. [22,24]. According to the Atiyah-Singer index theorem [29–32], the zero modes of the Dirac operator are related to the topological charges. Any source of topological charge can attract (would-be) zero modes, which contribute via interactions in Monte Carlo simulations to a finite density of near-zero modes. By the Banks-Casher relation [33], the finite density of near-zero modes leads to a nonzero chiral condensate and therefore chiral symmetry breaking. For studying the contributions of different types of topological charge sources of center vortices and analyzing low-lying modes of the Dirac operator for vortex configurations with these topological charge sources, it is necessary to consider special vortex configurations. The color structures and intersection points of center vortices producing the topological charge may appear on the vacuum, simultaneously.

In this article, we study some plane vortex configurations in SU(2) lattice gauge theory, which are combinations of the color structures and intersection points. These configurations give the nice opportunity to study the properties of zero modes and near-zero modes. On periodic lattices,

plane vortices appear in parallel or antiparallel pairs. By combining two perpendicular vortex pairs and making one of the plane vortices colorful, we get some configurations in which the intersection points and color structures are apart. Various topological charge contributions of the color structures and intersection points are studied in these configurations. We calculate eigenvalues and low-lying eigenmodes of the overlap Dirac operator in the background of the considered vortex configurations, and the chiral properties of the low-lying eigenmodes are analyzed.

This paper is organized as follows. In Sec. II, we describe the planar vortex configurations. Combinations of intersections and colorful regions and topological charges of these vortex configurations are investigated in Sec. III. Then, in Sec. IV, we study eigenvalues and eigenmodes of the overlap Dirac operator for the vortex configurations and analyze the influence of combinations of intersection points and colorful regions on low-lying modes of the Dirac operator. In the last step, Sec. V, we summarize the main points of our study.

## II. THICK PLANAR VORTEX CONFIGURATIONS

In SU(2) lattice gauge theory, we investigate thick plane vortices [20,25], which are parallel to two of the coordinate axes and occur in pairs of parallel sheets because of using periodic boundary conditions for the gauge fields. We use vortex plane pairs which extend in  $zt$  and  $xy$  planes. The lattice links of plane vortices as an unicolor vortex field vary in a  $U(1)$  subgroup of SU(2) and usually are defined by the Pauli matrix  $\sigma_3$ , i.e.,  $U_\mu = \exp\{i\alpha\sigma_3\}$ . For  $xy$  vortices ( $zt$  vortices),  $t$  links ( $y$  links) are nontrivial in one  $t$  slice  $t_\perp$  ( $y$  slice  $y_\perp$ ). The orientation of the vortex flux is determined by the gradient of the angle  $\alpha$ , which is chosen as a linear function of the coordinate perpendicular to the plane vortices. For  $xy$  vortices, the appropriate profile functions for angle  $\alpha$  are given as the following:

\*smhosseininejad@ut.ac.ir

*Published by the American Physical Society under the terms of the Creative Commons Attribution 4.0 International license. Further distribution of this work must maintain attribution to the author(s) and the published article's title, journal citation, and DOI. Funded by SCOAP<sup>3</sup>.*

$$\alpha_1(z) = \begin{cases} 2\pi \\ \pi[2 - \frac{z-(z_1-d)}{2d}] \\ \pi \\ \pi[1 - \frac{z-(z_2-d)}{2d}] \\ 0 \end{cases} \dots \alpha_2(z) = \begin{cases} 0 & 0 < z \leq z_1 - d \\ \frac{\pi}{2d}[z - (z_1 - d)] & z_1 - d < z \leq z_1 + d \\ -\pi & z_1 + d < z \leq z_2 - d \\ -\pi[1 - \frac{z-(z_2-d)}{2d}] & z_2 - d < z \leq z_2 + d \\ 0 & z_2 + d < z \leq N_z \end{cases} \quad (2.1)$$

The parallel sheets of  $xy$  vortices have thickness of  $2d$  centered around  $z_1$  and  $z_2$ . Vortex pairs with the same (opposite) vortex flux orientation corresponding to the angle  $\alpha_1$  ( $\alpha_2$ ) are called parallel (antiparallel) vortices. It should be noted that the unicolor vortices defined with Eq. (2.1) are not thickened in both transverse dimensions; an  $xy$  vortex is thick in the  $z$  direction but still thin in the  $t$  direction. Thus, these vortices resemble bands rather than tubes. The vortex profiles  $\alpha(x)$  similar to Eq. (2.1) are used for  $zt$  vortices centered around  $x_1$  and  $x_2$ . A  $zt$  vortex is thick in the  $x$  direction but still thin in the  $y$  direction.

The topological charge of the configurations on the continuum is defined as

$$Q = \int d^4x q(x) = -\frac{1}{16\pi^2} \int d^4x \text{tr}[\tilde{\mathcal{F}}_{\mu\nu} \mathcal{F}_{\mu\nu}], \quad (2.2)$$

where  $q(x)$  denotes topological charge density,  $\tilde{\mathcal{F}}_{\mu\nu} = \frac{1}{2}\epsilon_{\mu\nu\alpha\beta}\mathcal{F}_{\alpha\beta}$ ,  $\mathcal{F}_{\mu\nu} = -igF_{\mu\nu}$ ,  $F_{\mu\nu} = F_{\mu\nu}^a \frac{\sigma^a}{2}$ , and  $F_{\mu\nu}^a = \partial_\mu A_\nu^a - \partial_\nu A_\mu^a + gf_{abc}A_\mu^b A_\nu^c$ . The plaquette definition discretizes the continuum expression [34–37]. The trace evaluates to

$$\text{tr}[\tilde{\mathcal{F}}_{\mu\nu} \mathcal{F}_{\mu\nu}] = (-2g^2)[F_{12}^a F_{34}^a - F_{13}^a F_{24}^a + F_{14}^a F_{23}^a]. \quad (2.3)$$

The field tensor  $F_{\mu\nu}$  is obtained from the plaquette variables  $U_{\mu\nu} = U_\mu(x)U_\nu(x+\mu)U_\mu^\dagger(x+\nu)U_\nu^\dagger(x)$  as

$$U_{\mu\nu}(x) \approx \exp\left[ia^2 g F_{\mu\nu}^b(x) \frac{\sigma^b}{2}\right]. \quad (2.4)$$

If a plaquette is written as

$$U_{\mu\nu}(x) = u_{\mu\nu}^0(x)I + iu_{\mu\nu}^b(x)\sigma^b, \quad (2.5)$$

one can obtain

$$F_{\mu\nu}^b = \frac{2}{a^2 g} u_{\mu\nu}^b(x). \quad (2.6)$$

To define a field tensor  $F_{\mu\nu}$  for a single lattice point, we average over the four adjacent plaquettes in the forward and backward directions. This means in the above expressions we make the substitution

$$U_{\mu\nu}(x) \rightarrow \tilde{U}_{\mu\nu}(x) = \frac{1}{4} \sum U_{\pm\mu, \pm\nu}(x). \quad (2.7)$$

Combining Eqs. (2.2), (2.3), and (2.6), the lattice topological charge density is [37]

$$q(x) = \frac{1}{2\pi^2 a^4} [\tilde{u}_{12}^a \tilde{u}_{34}^a - \tilde{u}_{13}^a \tilde{u}_{24}^a + \tilde{u}_{14}^a \tilde{u}_{23}^a], \quad (2.8)$$

where  $\tilde{u}_{\mu\nu}$  are the components of  $\tilde{U}_{\mu\nu}$ . Therefore, the lattice topological charge is obtained as

$$Q = a^4 \sum_x q(x). \quad (2.9)$$

For the plane vortices as the unicolor vortex fields, one gets vanishing gluonic topological charge. The color structure and intersection points of the plane vortices can contribute to the topological charge.

Each intersection between  $xy$  and  $zt$  vortices carries a topological charge with modulus  $|Q| = 1/2$ , the sign of which depends on the relative orientation of the vortex fluxes [20].

A colorful region of the  $xy$  vortex with radius  $R$  around  $(x_0, y_0)$  at  $z_1$  and  $t_\perp$  is defined by the timelike links  $\exp\{ia\vec{n}\vec{\sigma}\}$  distributed over the full  $SU(2)$  gauge group [22]. The color direction  $\vec{n}$  is

$$\vec{n} = \sin(\theta(\rho)) \cos(\phi) \hat{i} + \sin(\theta(\rho)) \sin(\phi) \hat{j} + \cos(\theta(\rho)) \hat{k}, \quad (2.10)$$

where

$$\begin{aligned} \rho &= \sqrt{(x-x_0)^2 + (y-y_0)^2}, \\ \theta(\rho) &= \pi \left(1 - \frac{\rho}{R}\right) H(R-\rho) \in [0, \pi], \\ \phi &= \arctan \frac{y-y_0}{x-x_0} \in [0, 2\pi). \end{aligned} \quad (2.11)$$

$H$  is the Heaviside step function. For the colorful configuration as defined up to this point, one obtains a vanishing gluonic topological charge [22], but this can be seen to represent a lattice artifact. By a gauge transformation, one can show that the colorful configuration represents a fast

transition between two vacua with different winding numbers in the temporal direction (sharp vortices) [22,28]. After smoothing the colorful vortices by growing the temporal extent  $\Delta t$  of the configuration, the topological charge of the configuration becomes nonzero. The topological charge of the smoothed configuration obtains modulus  $|Q| = 1$ , the sign of which depends on the profile of the colorful vortex sheet. Therefore, for the colorful vortices, it turns out to be quite crucial to thicken in both transverse dimensions, and vanishing of the topological charge of the sharp vortices ( $\Delta t = 1$ ) is a lattice artifact due to the singularity of the vortex in temporal direction.

In the following, we study combinations of the color structure and intersection points of center vortices.

### III. COMBINATIONS OF COLORFUL REGIONS AND INTERSECTIONS POINTS

The color structures and intersection points of center vortices may appear on the vacuum, simultaneously. By combining these sources of topological charge, we investigate the influence of these combinations on low-lying modes of the Dirac operator. According to the topological charge definition

$$Q = -\frac{1}{32\pi^2} \int d^4x \epsilon_{\mu\nu\alpha\beta} \text{tr}[\mathcal{F}_{\alpha\beta} \mathcal{F}_{\mu\nu}] = \frac{1}{4\pi^2} \int d^4x \vec{E}^a \cdot \vec{B}^a, \quad (3.1)$$

when a configuration has electric and magnetic fields, it can contribute to the topological charge. The index  $a$  is related to the three directions  $\sigma_a$  of the SU(2) color algebra. The unicolor regions of plane vortices, as explained in the previous section, are defined by the Pauli matrix  $\sigma_3$ . The unicolor region of  $xy$  vortices has only nontrivial  $zt$  plaquettes and therefore an electric field  $E_z^3$ , while the one of the  $zt$  vortices bears nontrivial  $xy$  plaquettes and therefore a magnetic field  $B_z^3$ . The topological charge of an intersection point between  $xy$ - and  $zt$ -vortex sheets is then proportional to  $E_z^3 B_z^3$ . The intersection points with the same (opposite) orientation of  $xy$ - and  $zt$ -vortex fluxes are parallel (anti-parallel) crossings, and their topological charge contribution is  $Q = 1/2$  ( $Q = -1/2$ ).

For the colorful regions, three directions of  $\sigma_a$  contribute to the topological charge, while for the intersection points, one direction of  $\sigma_a$  contributes to the topological charge.

Now, we study some configurations in which the colorful regions and intersection points are combined. In the configurations,  $xy$  vortices which have the color structures are thickened in both transverse dimensions, but  $zt$  vortices are thickened in the  $x$  direction but still thin in the  $y$  direction.

For the first step, we intersect a parallel  $xy$ -vortex pair at  $(z_1 = 4, z_2 = 14)$  with a parallel  $zt$ -vortex pair at  $(x_1 = 4, x_2 = 14)$  with thickness  $d = 2$  at  $(t_\perp = 3, y_\perp = 9)$  on a  $16^4$  lattice. We use  $\alpha_1$ , given in Eq. (2.1), as the angle profile of

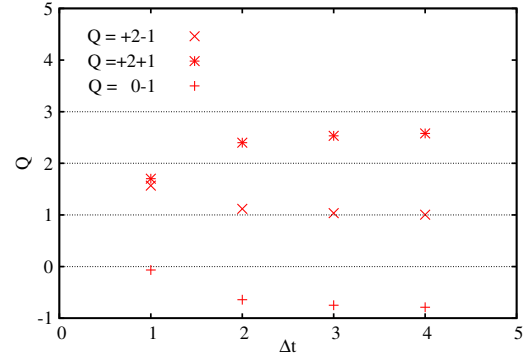


FIG. 1. The total topological charge of some vortex configurations corresponding to Fig. 2, which are combinations of colorful region and intersection points. In the figure, topological charge  $Q$  of any configuration is  $Q_{\text{int}} + Q_{\text{col}}$ , the sum of intersection and colorful contributions. For the configurations as the fast transition in temporal direction ( $\Delta t = 1$ ), the topological charge contribution of colorful region does not appear due to the singularity of the configuration in temporal direction. After growing the temporal extent of the configurations, the topological charge contribution of the colorful region is added.

the vortex pairs. The colorful region with radius  $R = 4$  is located in the first vortex sheet of the  $xy$ -plane vortices ( $z_1 = 4$ ) with the center at  $x_0 = y_0 = 9$  in the  $xy$  plane. The intersection points and the colorful region are apart. However, there is a quite small overlap between these regions, which has only a minor effect. Note that the radius of the colorful region and the thickness of vortex sheets should be appropriate for obtaining the Dirac modes. In Fig. 1, the topological charge of the configuration is plotted for various values of  $\Delta t$ . In the plot, the  $Q$  symbol is composed of  $Q_{\text{int}} + Q_{\text{col}}$ , the sum of topological charges of intersection and colorful contributions. As shown, for the sharp configuration where  $\Delta t = 1$ , the total charge contribution  $Q = 2$  of four intersection points appears. The topological charge after smoothing the configuration, where the charge contribution of color structure is added, approaches from  $Q = 2$  to  $Q = 2 - 1 = 1$ . The schematic diagram for the intersection plane of this configuration is shown in Fig. 2(a). Each intersection point and colorful region carry topological charge  $Q = +1/2$  and  $Q = -1$ , respectively. The minimum value of the action  $S$  as a function of  $\Delta t$  corresponding to the colorful region is  $1.68 S_{\text{inst}}$  around  $\Delta t = R$ , where the instanton action  $S_{\text{inst}} = 8\pi^2/g^2$  [22]. Therefore, we consider  $\Delta t = R$ , with our choice of  $R = 4$ , cf. above; the transition thus occurs between  $t = 1$  and  $t = 5$ . In Fig. 3(a), the topological charge density of the  $Q = 1$  configuration at  $(t_\perp = 3, y_\perp = 9)$  is plotted in the  $xz$  plane (the intersection plane), where we can identify the positive and negative contributions indicated in Fig. 2(a).

For the next step, we consider a configuration that is the same as the first configuration but with the angle profile of the vortex pairs being  $-\alpha_1$ . The parameters for this vortex

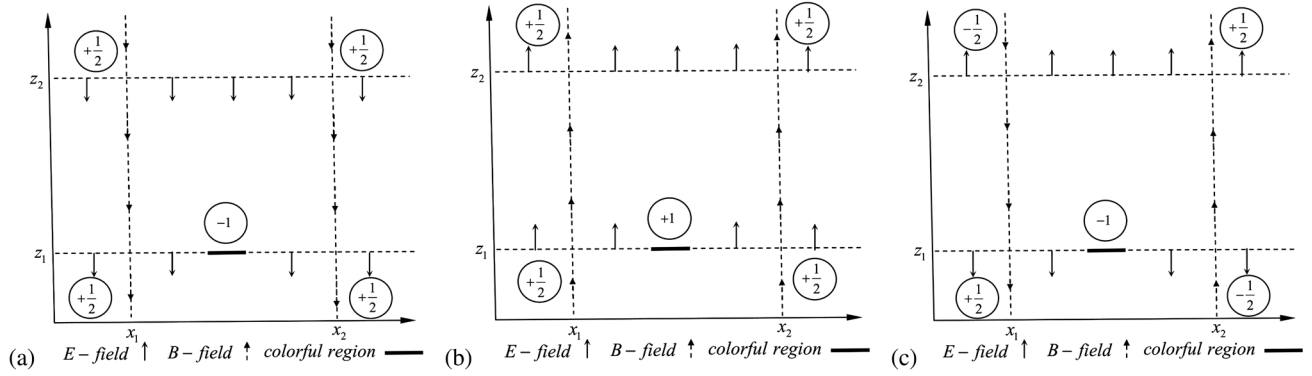


FIG. 2. The geometry, field strength, and topological charge contributions of the intersection points and colorful region in the intersection plane. The bold black line indicates that the unicolor vortex is substituted in this region by a colorful region. (a)  $Q = 1$  configuration in which two parallel vortex pairs are intersected. We use  $\alpha_1$  as the angle profile of the vortex pairs. The total topological charge contribution of intersection points is  $Q = 2$ , and the one of colorful region is  $Q = -1$ . Therefore, various contributions sum up to a total topological charge  $Q = 1$ . (b)  $Q = 3$  configuration which is the same as  $Q = 1$  configuration but the angle profile of the vortex pairs is  $-\alpha_1$ . The total topological charge contribution of intersection points is  $Q = 2$ , and the one of colorful region is  $Q = 1$ . Therefore, various contributions sum up to a total topological charge  $Q = 3$ . (c)  $Q = -1$  configuration in which two antiparallel vortex pairs are intersected. We use  $\alpha_2$  as the angle profile of the vortex pairs. The total topological charge contribution of intersection points is  $Q = 0$ , and the one of colorful region is  $Q = -1$ . Therefore, various contributions sum up to a total topological charge  $Q = -1$ .

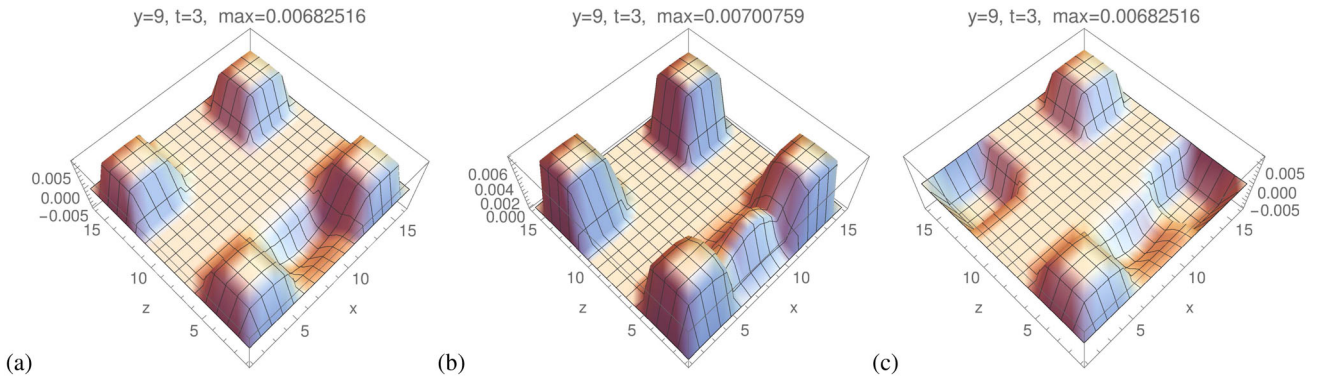


FIG. 3. The topological charge densities in the  $xz$  plane for the configurations displayed in Fig. 2, which are two intersecting  $xy$ - and  $zt$ -plane vortex pairs with vortex centers  $(z_1 = 4, z_2 = 14)$  and  $(x_1 = 4, x_2 = 14)$  at  $(t_\perp = 3, y_\perp = 9)$  with thickness  $d = 2$  and  $\Delta t = R = 4$  on a  $(16)^4$  lattice. The color structure of the  $xy$  vortices is located in the first vortex sheet ( $z_1 = 4$ ), and the vacuum to vacuum transition occurs between  $t = 1$  and  $t = 5$ . The center of the colorful region is located at  $x_0 = y_0 = 9$  in the  $xy$  plane.

configuration are the same as those of the  $Q = 1$  configuration. As shown in Fig. 1, for the sharp configuration, the total charge contribution  $Q = 2$  of four intersection points appears. The topological charge after smoothing the configuration approaches from  $Q = 2$  to  $Q = 2 + 1 = 3$ . The schematical diagram for the intersection plane of this configuration is shown in Fig. 2(b). Each intersection point and colorful region carry topological charge  $Q = +1/2$  and  $Q = +1$ , respectively. In Fig. 3(b), the topological charge density of the  $Q = 3$  configuration at  $(t_\perp = 3, y_\perp = 9)$  is plotted in the intersection plane, where we can identify the positive contributions indicated in Fig. 2(b).

For the last step, we intersect two antiparallel vortex pairs. The parameters for this vortex configuration are the same as those of the  $Q = 1$  configuration, and the angle

profile of the vortex pairs is  $\alpha_2$ , given in Eq. (2.1). As shown in Fig. 1, for the sharp configuration, the total charge contribution  $Q = 0$  of four intersection points appears. The topological charge after smoothing the configuration approaches from  $Q = 0$  to  $Q = 0 - 1 = -1$ . The schematical diagram for the intersection plane of this configuration is shown in Fig. 2(c). Two of the intersection points carry topological charge  $Q = +1/2$ , while the other two intersection points have  $Q = -1/2$ , and the colorful region carries topological charge  $Q = -1$ . They sum up to total topological charge  $Q = -1$ . In Fig. 3(c), the topological charge density of the  $Q = -1$  configuration at  $(t_\perp = 3, y_\perp = 9)$  is plotted in the intersection plane, where we can identify the positive and negative contributions indicated in Fig. 2(c).

In the next section, we analyze the low-lying modes of the overlap Dirac operator in the background of these vortex configurations.

#### IV. FERMIONIC DIRAC MODES FOR THE VORTEX FIELDS

In the previous section, we defined some vortex configurations which are combinations of the color structures and intersection points. For studying the effect of these configurations on fermions  $\psi$ , we determine the low-lying chiral eigenvectors  $\chi_{R,L}$  and eigenvalues  $|\lambda| \in [0, 2/a]$  of the overlap Dirac operator [38–41]

$$D_{ov} = \frac{1}{a} \left[ 1 + \gamma_5 \frac{H}{|H|} \right] \quad \text{with} \quad H = \gamma_5 A, \quad (4.1)$$

$$A = aD_W - m,$$

where  $D_W$  denotes the massless Wilson Dirac operator [42,43]. The mass parameter  $m$ , which is in the range  $(0,2)$ , is chosen with  $m = 1$ , and the lattice constant  $a$  is set to  $a = 1$ . The eigenvalues of the overlap Dirac operator as a Ginsparg-Wilson operator are restricted to a circle in the complex plane. This circle crosses the real axis at the two points  $\lambda = 0$  and  $\lambda = 1$  (doubler modes). Zero and doubler modes have exact chirality; i.e., they are eigenvectors of  $\gamma_5$ . The eigenvalues  $|\lambda| \in (0, 2/a)$  come in complex conjugate pairs. Both of the eigenvectors  $\psi_{\pm} = \frac{1}{\sqrt{2}}(\chi_R \pm i\chi_L)$  belonging to one value of  $|\lambda| \neq 0, 2/a$  have the same chiral density as

$$\chi = \psi_{\pm}^{\dagger} \gamma_5 \psi_{\pm} = \frac{1}{2} (\chi_R^{\dagger} \chi_R - \chi_L^{\dagger} \chi_L). \quad (4.2)$$

According to the Atiyah-Singer index theorem, the topological charge has to be related to zero modes of the Dirac operator by  $\text{ind}D[A] = n_- - n_+ = Q$ , where  $n_-$  and  $n_+$  denote the numbers of left- and right-handed zero modes [29–32]. For a single configuration, one never finds fermionic zero modes of both chiralities. It means that for a gauge field with nonvanishing topological charge  $Q$  the overlap Dirac operator  $D_{ov}$  has  $|Q|$  exact zero modes with chirality  $-\text{sign}Q$ . Therefore, any source of topological charge can attract zero modes contributing through interactions to a finite density of near-zero modes leading to chiral symmetry breaking via the Banks-Casher relation.

As mentioned above, we defined the  $Q = 1$  ( $Q = 3$ ) configuration, which is two intersecting parallel vortex pairs where one of the vortices is colorful, negatively (positively) charged, and also the  $Q = -1$  configuration, which is two intersecting antiparallel vortex pairs where one of the vortices is colorful, negatively charged.

In Fig. 4, we show the lowest eigenvalues of the overlap Dirac operator in the background of these configurations compared to the eigenvalues of the free overlap Dirac

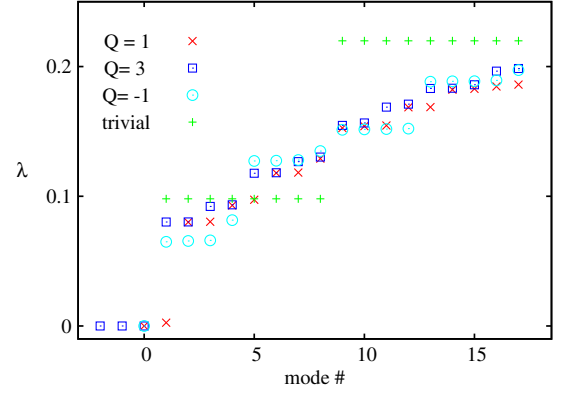


FIG. 4. The lowest overlap eigenvalues for the vortex configurations schematically depicted in Fig. 2 with  $Q = 1$  [Fig. 2(a)],  $Q = 3$  [Fig. 2(b)], and  $Q = -1$  [Fig. 2(c)], compared with those of the free Dirac operator on a  $16^4$  lattice.

operator. For the fermion fields, we use antiperiodic boundary conditions in the temporal direction and periodic boundary conditions in spatial directions on a  $16^4$  lattice. The parameters of the configurations are the same as those in the previous section (given in Fig. 3). For better comparison, we indicate the Dirac modes with mode number  $\#(m)$  ( $m \leq 0$  means zero modes, and  $m > 0$  would be nonzero modes). As shown in Fig. 4, we find one zero mode  $\#(0)$  of negative chirality for the  $Q = 1$  configuration; three zero modes  $\#(-2)$ ,  $\#(-1)$ , and  $\#(0)$  of negative chirality for the  $Q = 3$  configuration; and one zero mode  $\#(0)$  of positive chirality for the  $Q = -1$  configuration, as expected from the index theorem. As shown in Fig. 4, we also get one near-zero mode  $\#(1)$  for the  $Q = 1$  configuration. The near-zero mode  $\#(1)$  is distinguished from the mode  $\#(0)$  by the chirality properties, making it a near-zero mode as opposed to a zero mode.

Now, we study the properties of zero modes and near-zero modes. In Figs. 5 and 6, we show the chiral densities of the zero modes for these configurations. The plot titles in the density plots indicate the plane positions, the chirality [“chi = 0” means we plot  $\chi$ , given in Eq. (4.2); “chi = 1” would be the right-handed chiral density  $\chi = \frac{1}{2}(\chi_R^{\dagger} \chi_R)$ ; and “chi = -1” is the left-handed chiral density  $\chi = \frac{1}{2}(\chi_L^{\dagger} \chi_L)$ ], and the number  $n$  is related to the plotted mode  $\#(n)$  and the maximal density in the plotted area, “max = ...”

For the  $Q = 1$  configuration, the total topological charge is a combination of  $Q = 2$  (intersection contributions) and  $Q = -1$  (color structure contribution). As shown in Fig. 5(a), the chiral density  $\chi(\#0)$  of the zero mode for the  $Q = 1$  configuration shows four distinct maxima near to the intersection points. Although there is the colorful region in the configuration, it does not attract the chiral density  $\chi(\#0)$  of the zero mode anymore.

For the  $Q = -1$  configuration, the total topological charge is a combination of  $Q = 0$  (intersection contributions) and  $Q = -1$  (color structure contribution). As shown

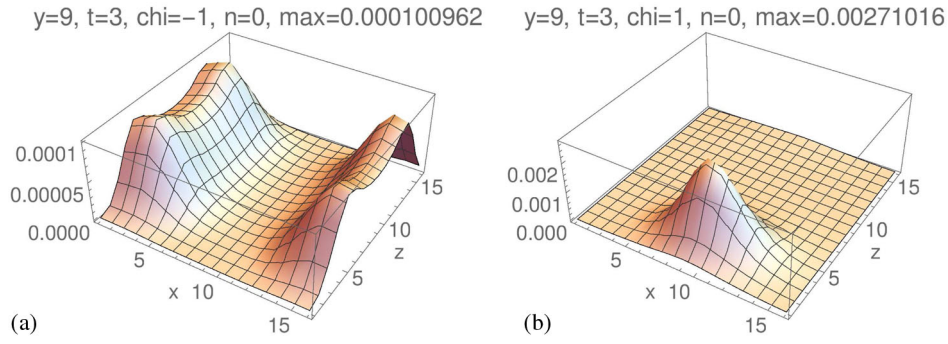


FIG. 5. The chiral density  $\chi(x)$  of the zero mode (a) for the  $Q = 1$  configuration and (b) for the  $Q = -1$  configuration in the  $xz$  plane. For the  $Q = 1$  configuration, the chiral density of the zero mode shows four distinct maxima near to the intersection points. The colorful region in the configuration does not attract the chiral density of the zero mode anymore. For the  $Q = -1$  configuration, the chiral density of the zero mode is localized in the colorful region.

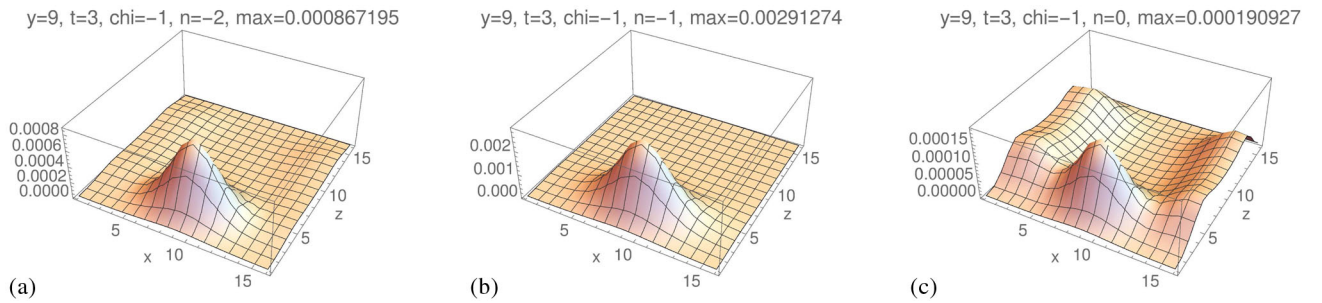


FIG. 6. The chiral densities of three zero modes for the  $Q = 3$  configuration. The chiral densities of the zero modes peak at the center of the colorful region. Two zero modes  $\#(-2)$  and  $\#(-1)$  are concentrated completely on the colorful region, and one zero mode  $\#0$  is on both the intersection and colorful regions.

in Fig. 5(b), the chiral density  $\chi(\#0)$  of the zero mode for the  $Q = -1$  configuration is localized in the colorful region.

For the  $Q = 3$  configuration, the total topological charge is a combination of  $Q = 2$  (intersection contributions) and  $Q = 1$  (color structure contribution). In Fig. 6, we show the chiral densities of three zero modes for the  $Q = 3$  configuration. Although a naive identification of topological and chiral densities would suggest that there should be one zero mode concentrated on the colorful region and two on the intersection points, a quite different distribution is in fact observed. As shown, the chiral densities of the zero modes peak at the center of the colorful region. Two zero modes  $\#(-2)$  and  $\#(-1)$  are concentrated completely on the colorful region, and one zero mode  $\#0$  is on both the intersection and colorful regions.

The index theorem may mislead one to identify topological densities with chiral densities and deduce from the location of the chiral density where topological density should be assigned. However, the index theorem is only a statement about integrated densities, not the densities themselves. The densities cannot be identified one to one.

Considering Figs. 5 and 6 together, it seems that one can conclude that zero modes are correlated more strongly with the colorful vortex region than with the intersection points

whenever the chirality of the zero mode can match the sign of either of those regions of topological charge. Only in the case of Fig. 5(a) where the chirality of the zero mode merely matches the sign of the topological charge due to the intersection points, the zero mode remains attached to the intersection points.

Now, we study the low-lying modes of the considered vortex configurations after zero modes. As mentioned above, we find one near-zero mode  $\#(1)$  for the  $Q = 1$  configuration. For the  $Q = 1$  configuration, the total topological charge is a combination of  $Q = 2$  (intersection contributions) and  $Q = -1$  (color structure contribution). The Dirac operator in the background of this configuration has one negative chirality zero mode (tied to a positive, intersection, contribution  $Q = 1$ ) and two would-be zero modes (for another intersection contribution  $Q = 1$  and the color structure contribution  $Q = -1$ ). The near-zero mode of the  $Q = 1$  configuration, as shown in Fig. 4, originates from the overlap of these two would-be zero modes. The left-handed chiral density  $\chi(\#1)$  ( $\text{chi} = -1$ ) of the near-zero mode behaves similarly to the chiral density ( $\text{chi} = -1$ ) of the zero mode  $\chi(\#0)$  for the configuration  $Q = +1$  [see Fig. 5(a)]. The right-handed chiral density  $\chi(\#1)$  ( $\text{chi} = 1$ ) of the near-zero mode behaves similarly to the chiral density ( $\text{chi} = 1$ ) of the zero mode  $\chi(\#0)$  for the

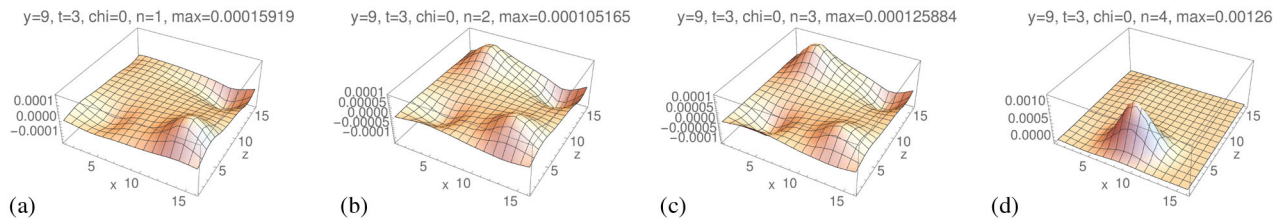


FIG. 7. The chiral densities of four low-lying modes after one zero mode for the  $Q = -1$  configuration. The first three chiral densities (a), (b), and (c) are localized near intersection points. (d) The fourth mode is localized near the colorful region.

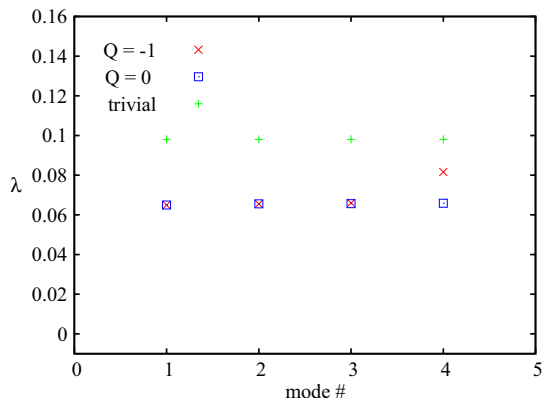


FIG. 8. The four low-lying eigenvalues for the  $Q = -1$  and  $Q = 0$  configurations compared with those of the free Dirac operator. For the  $Q = 0$  configuration, two antiparallel vortex pairs are intersected. The  $Q = -1$  configuration is the same as the  $Q = 0$  configuration, but we have added to the configuration the colorful region with  $Q = -1$ . The eigenvalues of the first three eigenmodes for the  $Q = 0$  configuration are the same as those of  $Q = -1$  configuration. The eigenvalue of the fourth low-lying mode of the  $Q = 0$  configuration is increased after locating within the colorful region.

$Q = -1$  configuration [see Fig. 5(b)]. As a result, the left-handed chiral density of the near-zero mode spreads near four intersection points, while the right-handed chiral density of the near-zero mode is localized near the colorful region.

Now, for the  $Q = -1$  configuration, we study four low-lying modes, #1), #2), #3), and #4), as shown in Fig. 4. For the  $Q = -1$  configuration, the total topological charge is a combination of  $Q = 0$  (intersection contributions) and  $Q = -1$  (color structure contribution). The  $Q = 0$  configuration, as an intersecting unicolor center vortex field with  $Q = 0$ , has been studied in Ref. [20], in which two of the intersection points carry topological charge  $Q = +1/2$  while the other two intersection points have  $Q = -1/2$ . Two antiparallel vortex pairs are intersected similarly to the  $Q = -1$  configuration, but we do not have the colorful region. For the  $Q = 0$  configuration, the first four low-lying modes are localized at intersection points. The chiral densities of four low-lying modes  $\chi(\#1)$ ,  $\chi(\#2)$ ,  $\chi(\#3)$ , and  $\chi(\#4)$  of the  $Q = -1$  configuration are shown in Fig. 7. The chiral densities of the three low-lying modes  $\chi(\#1)$ ,

$\chi(\#2)$ , and  $\chi(\#3)$  are localized at intersection points, while  $\chi(\#4)$  (fifth mode) is localized in the colorful region. In Fig. 8, the eigenvalues of these four low-lying modes of the  $Q = -1$  configuration are compared with those of the  $Q = 0$  configuration. The low-lying modes #1), #2), and #3) for both configurations have the same eigenvalues, while the eigenvalue of the low-lying mode #4) is increased compared with the one of the fourth low-lying mode of the  $Q = 0$  configuration. Therefore, the eigenvalue of mode #4) of the analogous  $Q = 0$  configuration is increased through the influence of the colorful region. It is possible that there is a level crossing and mode #4) of the  $Q = 0$  configuration, after distortion by the colorful region, becomes a higher mode of the  $Q = -1$  configuration.

## V. CONCLUSION

Understanding the dynamical mechanism of the spontaneous breaking of chiral symmetry in QCD is our aim. We analyze special vortex configurations which are combinations of intersection points and colorful regions for studying the properties of low-lying modes of the Dirac operator. We construct vortex configurations by combining two perpendicular plane vortex pairs and making one of the plane vortices colorful. The intersection points and the colorful region are apart. Our special vortex configurations have total topological charges  $Q = \pm 1$  and  $Q = 3$ . The  $Q = 1$  ( $Q = 3$ ) configuration is two intersecting parallel vortex pairs in which one of the vortices is colorful, negatively (positively) charged, and also the  $Q = -1$  configuration is two intersecting antiparallel vortex pairs in which one of the vortices is colorful, negatively charged.

These configurations give the nice opportunity to study the properties of zero modes and near-zero modes of the overlap Dirac operator. We have analyzed the low-lying modes of the overlap Dirac operator in the background of these configurations. The data provide insight, in particular, into the interplay between chiral densities induced by vortex intersection points and by color structure.

For the  $Q = 1$  configuration, we find one zero mode of negative chirality and one near-zero mode. The chiral density of the zero mode shows four distinct maxima near to the intersection points. The chirality of the zero mode only matches the sign of the topological charge due to intersection points; the zero mode remains attached to the

intersection points. The Dirac operator in the background of this configuration also has two would-be zero modes (for another intersection contribution  $Q = 1$  and the color structure contribution  $Q = -1$ ). The near-zero mode originates from the overlap of these two would-be zero modes. The left-handed chiral density of the near-zero mode spreads near to four intersection points, while the right-handed chiral density of the near-zero mode is localized near to the colorful region.

For the  $Q = -1$  configuration, we find one zero mode of positive chirality. The chiral density of the zero mode is localized in the colorful region. For this configuration, the total topological charge is a combination of  $Q = 0$  (intersection contributions) and  $Q = -1$  (color structure contribution). For the analogous unicolor  $Q = 0$  configuration, the chiral densities of the first four low-lying modes are localized in the intersection points. For the  $Q = -1$  configuration, the chiral densities of three of the first four low-lying modes, after one zero mode, behave similarly, but the chiral density of the fourth mode is localized in the colorful region. The eigenvalue of this mode is increased compared to the fourth low-lying mode of the  $Q = 0$  configuration.

For the  $Q = 3$  configuration, we find three zero modes of negative chirality. Although a naive identification of topological and chiral densities would suggest that there should be one zero mode concentrated on the colorful region and two on the intersection points, a quite different distribution is in fact observed. The chiral densities of three zero modes peak at the center of the colorful region. Two zero modes are concentrated completely on the colorful region, and one zero mode is on both the intersection and colorful regions.

It seems that one can conclude that zero modes are correlated more strongly with the colorful vortex region than with the intersection points whenever the chirality of the zero mode can match the sign of either of those regions of topological charge.

Zero modes and near-zero modes of the type studied in this work may be instrumental in generating a nonzero spectral density of the Dirac operator near-zero eigenvalue and thus lead to spontaneous chiral symmetry breaking.

### ACKNOWLEDGMENTS

I am grateful to Manfred Faber, Roman Höllwieser, and Urs M. Heller to prepare the basic programs.

- 
- [1] L. Del Debbio, M. Faber, J. Greensite, and Š. Olejník, Center dominance and  $Z(2)$  vortices in  $SU(2)$  lattice gauge theory, *Phys. Rev. D* **55**, 2298 (1997).
  - [2] L. Del Debbio, M. Faber, J. Greensite, and S. Olejník, Center Dominance, Center Vortices, and Confinement, in *New Developments in Quantum Field Theory. Proceedings of the NATO Advanced Research Workshop*, NATO Science Series: B (Advanced Science Institutes Series) Vol. 366 (Springer, Boston, 2002).
  - [3] Tamas G. Kovacs and E. T. Tomboulis, Vortices and confinement at weak coupling, *Phys. Rev. D* **57**, 4054 (1998).
  - [4] J. Greensite, The confinement problem in lattice gauge theory, *Prog. Part. Nucl. Phys.* **51**, 1 (2003).
  - [5] P. Vinciarelli, Fluxon solutions in nonabelian gauge models, *Phys. Lett.* **78B**, 485 (1978).
  - [6] T. Yoneya,  $Z(N)$  topological excitations in Yang-Mills theories: Duality and confinement, *Nucl. Phys.* **B144**, 195 (1978).
  - [7] J. M. Cornwall, Quark confinement and vortices in massive gauge invariant QCD, *Nucl. Phys.* **B157**, 392 (1979).
  - [8] G. Mack and V. B. Petkova, Comparison of lattice gauge theories with gauge groups  $Z(2)$  and  $SU(2)$ , *Ann. Phys. (N.Y.)* **123**, 442 (1979).
  - [9] H. B. Nielsen and P. Olesen, A quantum liquid model for the QCD vacuum: Gauge and rotational invariance of domain and quantized homogeneous color fields, *Nucl. Phys.* **B160**, 380 (1979).
  - [10] P. de Forcrand and M. D'Elia, On the Relevance of Center Vortices to QCD, *Phys. Rev. Lett.* **82**, 4582 (1999).
  - [11] C. Alexandrou, P. de Forcrand, and Massimo D'Elia, The Role of center vortices in QCD, *Nucl. Phys.* **A663–664**, 1031c (2000).
  - [12] M. Engelhardt, Center vortex model for the infrared sector of Yang-Mills theory: Quenched Dirac spectrum and chiral condensate, *Nucl. Phys.* **B638**, 81 (2002).
  - [13] R. Höllwieser, M. Faber, J. f. Greensite, U. M. Heller, and S. Olejník, Center vortices and the Dirac spectrum, *Phys. Rev. D* **78**, 054508 (2008).
  - [14] H. Reinhardt and M. Engelhardt, *Center Vortices in Continuum Yang-Mills Theory*, Quark Confinement and the Hadron Spectrum, edited by W. Lucha and K. M. Maung (World Scientific, Singapore, 2002), Vol. IV, p. 150.
  - [15] H. Reinhardt, Topology of center vortices, *Nucl. Phys.* **B628**, 133 (2002).
  - [16] M. Engelhardt, Center vortex model for the infrared sector of Yang-Mills theory: Topological susceptibility, *Nucl. Phys.* **B585**, 614 (2000).
  - [17] R. Bertle, M. Engelhardt, and M. Faber, Topological susceptibility of Yang-Mills center projection vortices, *Phys. Rev. D* **64**, 074504 (2001).
  - [18] F. Bruckmann and M. Engelhardt, Writhe of center vortices and topological charge: An explicit example, *Phys. Rev. D* **68**, 105011 (2003).
  - [19] M. Engelhardt, Center vortex model for the infrared sector of  $SU(3)$  Yang-Mills theory: Topological susceptibility, *Phys. Rev. D* **83**, 025015 (2011).



- [20] R. Höllwieser, M. Faber, and U. M. Heller, Intersections of thick center vortices, Dirac eigenmodes and fractional topological charge in  $SU(2)$  lattice gauge theory, *J. High Energy Phys.* **06** (2011) 052.
- [21] R. Höllwieser and M. Engelhardt, Smearing center vortices, *Proc. Sci.*, LATTICE2014 (2015) 356.
- [22] S. M. Hosseini Nejad, M. Faber, and R. Höllwieser, Colorful plane vortices and chiral symmetry breaking in  $SU(2)$  lattice gauge theory, *J. High Energy Phys.* **10** (2015) 108.
- [23] R. Höllwieser and M. Engelhardt, Approaching  $SU(2)$  gauge dynamics with smeared  $Z(2)$  vortices, *Phys. Rev. D* **92**, 034502 (2015).
- [24] S. M. Hosseini Nejad and M. Faber, Colorful vortex intersections in  $SU(2)$  lattice gauge theory and their influences on chiral properties, *J. High Energy Phys.* **09** (2017) 068.
- [25] G. Jordan, R. Höllwieser, M. Faber, and U. M. Heller, Tests of the lattice index theorem, *Phys. Rev. D* **77**, 014515 (2008).
- [26] R. Höllwieser, M. Faber, and U. M. Heller, Spherical vortices, fractional topological charge and lattice index theorem in  $SU(2)$  LGT, *Proc. Sci.*, LATTICE2010 (2010) 276.
- [27] R. Höllwieser, M. Faber, and U. M. Heller, Critical analysis of topological charge determination in the background of center vortices in  $SU(2)$  lattice gauge theory, *Phys. Rev. D* **86**, 014513 (2012).
- [28] T. Schweigler, R. Höllwieser, M. Faber, and U. M. Heller, Colorful  $SU(2)$  center vortices in the continuum and on the lattice, *Phys. Rev. D* **87**, 054504 (2013).
- [29] M. F. Atiyah and I. M. Singer, The index of elliptic operators. 5, *Ann. Math.* **93**, 139 (1971).
- [30] A. S. Schwarz, On regular solutions of Euclidean Yang-Mills equations, *Phys. Lett.* **67B**, 172 (1977).
- [31] L. S. Brown, R. D. Carlitz, and C.-k. Lee, Massless excitations in instanton fields, *Phys. Rev. D* **16**, 417 (1977).
- [32] D. H. Adams, On the continuum limit of fermionic topological charge in lattice gauge theory, *J. Math. Phys. (N.Y.)* **42**, 5522 (2001).
- [33] T. Banks and A. Casher, Chiral symmetry breaking in confining theories, *Nucl. Phys.* **B169**, 103 (1980).
- [34] P. Di Vecchia, K. Fabricius, G. C. Rossi, and G. Veneziano, Preliminary evidence for  $U(1)$ -A breaking in QCD from lattice calculations, *Nucl. Phys.* **B192**, 392 (1981).
- [35] P. Di Vecchia, K. Fabricius, G. C. Rossi, and G. Veneziano, Numerical checks of the lattice definition independence of topological charge fluctuations, *Phys. Lett.* **108B**, 323 (1982).
- [36] R. Höllwieser, Ph.D. thesis, Vienna Technical University, Atominstitut, 2009.
- [37] G. Jordan, Ph.D. thesis, Vienna Technical University, Atominst., 2005.
- [38] R. Narayanan and H. Neuberger, Chiral Fermions on the Lattice, *Phys. Rev. Lett.* **71**, 3251 (1993).
- [39] R. Narayanan and H. Neuberger, A construction of lattice chiral gauge theories, *Nucl. Phys.* **B443**, 305 (1995).
- [40] H. Neuberger, Exactly massless quarks on the lattice, *Phys. Lett. B* **417**, 141 (1998).
- [41] R. G. Edwards, U. M. Heller, and R. Narayanan, A study of practical implementations of the overlap Dirac operator in four dimensions, *Nucl. Phys.* **B540**, 457 (1999).
- [42] K. G. Wilson, Confinement of quarks, *Phys. Rev. D* **10**, 2445 (1974).
- [43] C. Gattringer and C. B. Lang, Quantum chromodynamics on the lattice, *Lect. Notes Phys.* **788**, 1 (2010).